An electrochemical comparison of manganese dioxide microparticles *versus* α and β manganese dioxide nanorods: mechanistic and electrocatalytic behaviour

Christopher Batchelor-McAuley,[a] Lidong Shao,[b] Gregory G. Wildgoose,[a] Malcolm L. H. Green[b] and Richard G. Compton*[a]

Received (in Durham, UK) 7th December 2007, Accepted 31st January 2008
First published as an Advance Article on the web 21st February 2008
DOI: 10.1039/b718862e

The comparative electrochemical behaviour of both α- and β-nanorods of manganese dioxide (MnO_2) and microparticles of predominantly β-phase manganese dioxide is investigated at pHs close to neutral. In order to understand the observed voltammetric behaviour of all three materials the mechanisms of electrodeposition of MnO_2 onto a graphite electrode surface from a solution of Mn(II) at pH 3–7 is also reported. It is proposed that two competing mechanistic pathways operate, both invoking MnOOH as an intermediate species, which are an ECE or a DISP process, respectively. At low pH values (<pH 3) the mechanism likely proceeds *via* a DISP mechanism whereas at high pHs (pH ~ 7) the mechanism proceeds predominantly as an ECE process with the diffusion of protons out of the MnOOH intermediate being the likely rate determining step.

The α- and β-MnO_2 nanorods display a *ca.* 30 mV difference in the observed reduction potentials corresponding to a *ca.* 3 kJ mol^{-1} difference in the Gibb's energy between the two phases. There is also an observable difference in the reduction potential of the β-nanorods and β-microparticles, which probably reflects the differing surface or structural energies of the two materials. Finally the electrocatalytic performance of the three MnO_2 materials with respect to the analytical determination of hydrogen peroxide is investigated. Both phases of the MnO_2 nanorods exhibited a lower limit of detection (5.0 ± 2.5 μM based on 3σ) and greater sensitivity towards H_2O_2 than the MnO_2 microparticles, likely attributed to an increased surface area.

1. Introduction

Following Leclanché's invention of the zinc/manganese dioxide cell in 1864, MnO_2 has been used on a large scale in dry batteries.[1] High quality MnO_2 is required for battery production; a large proportion of which is produced electrochemically. Commonly the electrodeposition is done at low pHs and at a metal electrode. Subsequently an extensive number of investigations have focused on the electrochemical deposition of manganese dioxide in concentrated solutions of sulfuric acid and at platinum electrodes.[2–4] In modern alkaline batteries the MnO_2 cathode is bathed in a solution of KOH, as such the nature of MnO_2 at high pH values is also of great industrial interest.[5]

Within the last few years there has been an increasing amount of work done in attempting to produce manganese dioxide in a variety of novel forms such as nanorods or nanobelts.[6–9] This work has been undertaken with the main aim of producing improved cathodic materials for the use in batteries. As such most if not all of the electrochemical characterisation of these new substances has focused on their abilities as capacitors. These new forms of manganese dioxide are often one dimensional channel structures and are primarily made up of only one phase of manganese dioxide. The basic structural unit of many manganese oxides is an octahedron of oxygen coordinated to manganese, these octahedra can be linked along their edges and at their corners.[10] Alpha manganese dioxide (α-MnO_2) consists of 2 × 2 channels and is related to the mineral hollandite in structure, whereas beta manganese dioxide (β-MnO_2) consists of 1 × 1 channels and is similar in structure to the mineral pyrolusite.[1] It has been proposed by Grygar *et al.* that solid state voltammetry maybe used to differentiate between these differing structures in synthetic samples.[11]

It has also been known for a long time that manganese oxides possess interesting electrochemical properties. A large body of work has been focused on the use of manganese oxides of varying stoichometry (MnO_x) as highly selective heterogeneous catalyst materials. From this work oxides of manganese have found a wide range of uses within industry as catalysts for the photocatalytic oxidation of organic pollutants,[12] oxidation of carbon monoxide,[13] nitric oxide

[a] *Physical and Theoretical Chemistry Laboratory, Oxford University, South Parks Road, Oxford, UK OX1 3QZ. E-mail: richard.compton@chem.ox.ac.uk; Fax: +44 (0)1865 275410; Tel: +44 (0)1865 275413*
[b] *Inorganic Chemistry Laboratory, Oxford University, South Parks Road, Oxford, UK OX1 3QR*

reduction[14] and many more. But as noted by Langley *et al.* unsupported manganese oxide catalysts suffer from very low surface areas.[15]

Manganese is an essential element within biology with it present in many enzymes that involve the redox catalytic cycle of oxygen. Manganese even plays a role in photosynthesis with its involvement with photosystem II. As such it is a required micronutrient for many plants and cyanobacteria.[16] To the best of our knowledge only one paper so far deals with the deposition of manganese dioxide at neutral pH close to physiological pH. This work was done with the aim of producing a method for the trace analysis of manganese in natural waters.[17]

Enzymatic biosensors often produce hydrogen peroxide as the measurable analyte, this method has led to the effective low-potential amperometric detection of species such as lactate, phenols, alcohols and glucose.[18,19] The catalytic nature of manganese dioxide towards hydrogen peroxide, combined with the increased surface area of the manganese dioxide nanorods may provide a viable alternative method for the detection of hydrogen peroxide in place of the more commonly used electrode substrates.

Therefore this paper reports the catalytic properties at neutral pH of alpha- and beta-phase manganese dioxide nanorods in comparison to that of manganese dioxide microparticles, in conjunction with establishing a deeper understanding of how the catalytic process occurs and the electrochemical behaviour of this system at physiological pH by exploring the mechanism involved in the deposition of MnO_2.

2. Experimental

2.1 Reagents and equipment

All reagents were purchased from Aldrich (Gillingham, UK) and were used as received without further purification. All solutions were prepared using deionised water of resistivity not less than 18.2 MΩ cm at 298 K (Vivendi water systems, UK).

Electrochemical measurements were recorded using a computer controlled μAutolab potentiostat (EcoChemie) with a standard three electrode configuration in solutions containing 0.5 M NH_4NO_3 adjusted to pH 7.0 as the supporting electrolyte. The pH of the solution was measured using a pH213 Microprocessor pH meter (Hanna Instruments, Leighton Buzzard, UK). A basal plane pyrolytic graphite electrode (bppg, 5 mm diameter, Le Carbone, Sussex, UK) acted as the working electrode (see below). A platinum wire (99.99% GoodFellow, Cambridge, UK) counter electrode and a saturated calomel reference electrode (SCE, Radiometer, Copenhagen, Denmark) completed the cell assembly. The bppg electrode surface was renewed where necessary by pressing the electrode surface onto cellotape and gently peeling away the top few layers of graphite. Finally the bppg electrode was rinsed in acetone to remove any adhesive from the cellotape. All experiments were carried out at 20 ± 2 °C.

The crystallinity of the MnO_2 materials were analysed by use of a Panalytical XPert XRay diffractometer using copper K alpha1/alpha2 radiation in theta/theta geometry. The instrument has a programmable divergence slit with an XCelerator solid state detector.

The size and morphology of the produced MnO_2 nanorods were characterised using scanning electron microscopy (SEM) recorded using a JSM 6300 microscope, using an acceleration voltage of 20 kV and an operating distance of 15 mm.

2.2 Nanorod preparation

The preparation followed that given by Xu-Chun *et al.*[20] MnO_2 nanorods were synthesised under hydrothermal conditions. Experimental details were as follows: $MnSO_4$ (1.5 g) was dissolved in 10 ml of distilled water. 10 mL of aqueous solution containing 2.5 g of $KClO_3$ was then added to the above solution before being transferred into a Teflon-lined stainless steel autoclave (50 mL). The autoclave was sealed and maintained at either 150 °C or 220 °C for 12 h, to produce α-MnO_2 and β-MnO_2 nanorods, respectively. After the reaction was completed, the autoclave was allowed to cool to room temperature. The obtained brown powders were collected for characterisation.

2.3 Modification of a bppg electrode

In order to immobilise either α or β manganese dioxide nanorods onto the surface of a clean bppg electrode a "casting" solution of 1 mg/mL of each MnO_2 nanorod material suspended in methanol and sonicated for 5 minutes was used. A 20 μL aliquot of this casting suspension was then placed onto the bppg electrode surface and the solvent allowed to evaporate at room temperature leaving the MnO_2 nanorods immobilized onto the bppg surface. The MnO_2 microparticles were abrasively attached to the bppg electrode by rubbing the electrode surface on a filter paper containing a small amount of the manganese dioxide powder.

3. Results and discussion

3.1 Characterisation of the MnO_2 materials through XRD and SEM

Fig. 1(a) shows the XRD pattern for the MnO_2 microparticles, whilst Fig. 1(b) shows the XRD patterns for both the α-MnO_2 nanorods and the β-MnO_2 nanorods. The α-MnO_2 nanorods can be readily characterised by indexing the peaks present which show it to be a pure tetragonal phase of α-MnO_2 with lattice constants $a = 0.97847$ nm, $c = 0.28630$ nm.[20] Both the β-MnO_2 nanorods and the MnO_2 microparticles can also be characterised as being pure tetragonal phase β-MnO_2 with lattice constants $a = 0.43999$ nm, $c = 0.28740$ nm.[20]

The morphologies and sizes of the produced MnO_2 were investigated through the use of SEM. Fig. 2(a) shows a typical SEM image of the α-MnO_2 nanorods. As the nanorods were found to have diameters of 50–100 nm and lengths varying in the range of 3–5 μm. It can be seen from Fig. 2(b) that the produced β-MnO_2 did not comprise of just nanorods but also some larger rod like crystalline structures that have diameters up to 1 μm. The β-MnO_2 nanorods that were produced had diameters of 100–150 nm and lengths varying from 1–35 μm.

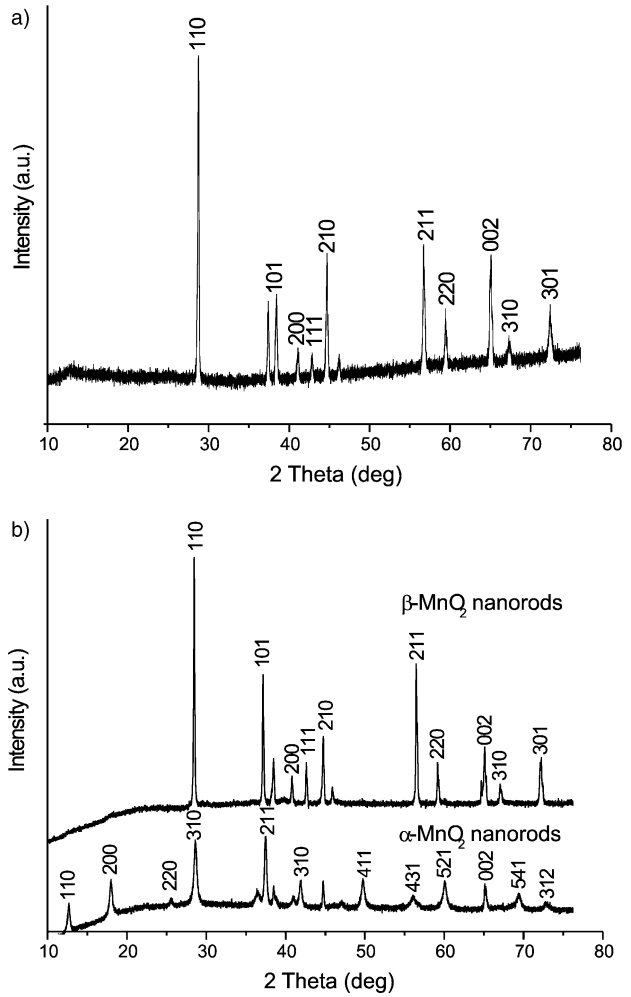

Fig. 1 (a) Shows the XRD pattern for the MnO_2 microparticles and (b) is the overlaid XRD patterns for the α-MnO_2 and β-MnO_2 nanorods.

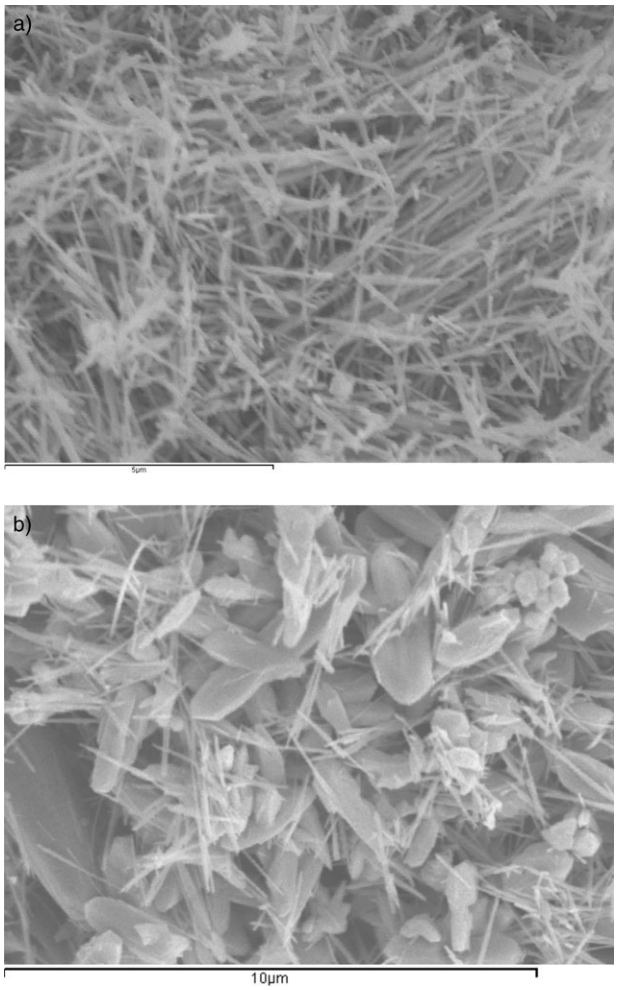

Fig. 2 The SEM images of (a) α-MnO_2 nanorods and (b) β-MnO_2 nanorods.

3.2 Voltammetric characterisation

The manganese dioxide samples were characterised by performing linear sweep voltammetry (LSV) in 0.1 M acetic acid +0.1 M sodium acetate adjusted to the desired pH by the addition of either HCl or NaOH. Fig. 3a and 3b show the cathodic stripping voltammetric behaviour of MnO_2 microparticles and the α-MnO_2 nanorods in the potential range of +1.2 V to +0.2 V (*vs.* SCE). The MnO_2 microparticles stripping peak varies by 126 mV per pH unit whereas the α-MnO_2 nanorods varied 114 mV per pH unit.

The variation of the stripping peak potential with pH was found to be in good agreement with that obtained by Saterlay *et al.* in which they show that the overall reduction is of manganese(IV) to manganese(II).[21]

$$MnO_2 + 4H^+ + 2e^- \rightarrow Mn^{2+} + 2H_2O \qquad (1)$$

Eqn (1) is a four proton two electron system and as such the peak potential is expected to shift by 118 mV per pH unit. This value is in close agreement to the values found experimentally for all the samples of MnO_2.

The standard potential for eqn (1) at pH 1.0 is $E^0 = +1.23$ V;[22] at pH 4.0 the calculated potential for the reduction of MnO_2 to Mn^{2+} is found to be +0.635 V (*vs.* SCE); this is in good agreement with the potential at which the experimental stripping peak is found (+0.628 V).

Fig. 4 shows the cathodic linear sweep voltammetry of MnO_2 microparticles in a pH 5.0 solution. The MnO_2 stripping peak appears at +0.53 V whilst a broad ill-defined peak is then observed at +0.1 V (*vs.* SCE). On repeat scans the size of the second peak diminishes greatly. A possible explanation for this voltammetric feature was proposed by Maskell and involved the formation of a thin layer of insulating MnOOH forming a Schottky-type barrier.[23]

Comparison of the position of the stripping peaks of the three different MnO_2 samples is shown in Fig. 5. The stripping peak for the β-MnO_2 nanorods occurs at a potential of +0.332 V (*vs.* SCE) whereas the corresponding peak for the α-MnO_2 nanorods occurs at a marginally higher potential of +0.363 V (*vs.* SCE). This difference in potential may be attributed to the change in Gibbs free energy between the two phases of MnO_2 if both phases exhibit electrochemically reversible behaviour, as appears to be the case from the Nernstian shift in peak potential with pH. Through the use

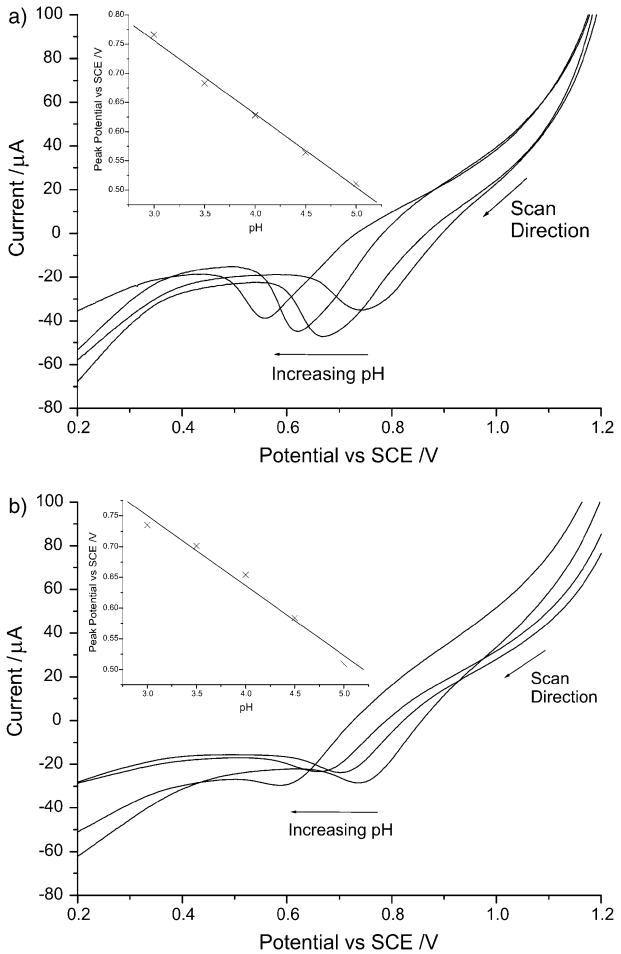

Fig. 3 The overlaid LSVs of a bppg electrode modified with (a) MnO_2 microparticles and (b) α-MnO_2 nanorods; in a solution of 0.1 M acetic acid +0.1 M sodium acetate adjusted to varying pH's with NaOH or HCl. LSV's ran at a scan rate of 100 mV/s. Insets shows the plot of peak position against pH.

of $\Delta G = -FE$ where F is the faraday constant and E is the potential difference then a value of 2.99 KJ mol^{-1} is found for the free energy difference between the two phases of the manganese dioxide nanorods. It has already been noted that the MnO_2 microparticles sample contains mainly beta-phase MnO_2. The stripping peak for the microparticles also occurs at a potential which is high than that for the β-MnO_2 nanorods. We speculate that this difference arises due to the increased structural energy of the nanometre-sized phase and as such it is reduced at a lower potential.

3.3 Mechanism of manganese dioxide electrodeposition from Mn^{2+}

As discussed in the introduction the mechanism by which MnO_2 is electrodeposited from solutions of Mn(II) has widely been studied at both low and high pH. However the mechanism has rarely been studied at neutral pH. As MnO_2 has often been purported to be an excellent substrate for the electrocatalytic detection of a variety of biologically active analytes such as H_2O_2,[24] ascorbic acid[25] (vitamin C) and nitrite,[15] we

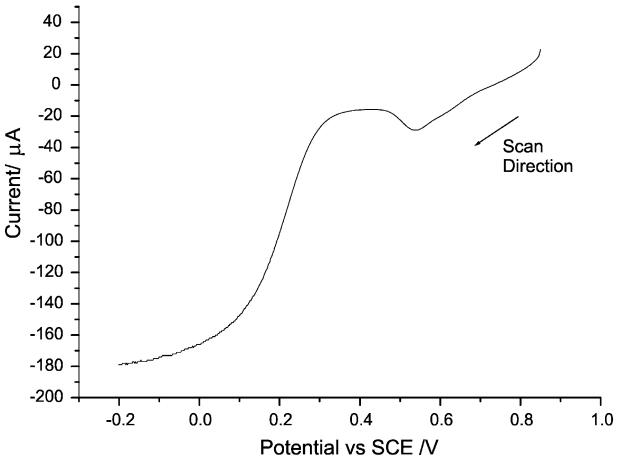

Fig. 4 The LSV of a bppg electrode modified with MnO_2 microparticles in a solution of 0.5 M NH_4NO_3 adjusted to pH 5.0 with 10 M NaOH. Scan swept in the cathodic direction from +0.85 V to −0.2 V (*vs.* SCE) at a scan rate of 100 mV/s.

now turn our attention to investigating the MnO_2 electrodeposition mechanism at pH's close to physiological pH. Our aim is to gain a thorough understanding of the electrochemical processes occurring in this system in order to apply that knowledge to the electrocatclytic detection of H_2O_2 and ascorbic acid at the α and β nanorods. For the majority of this work 0.5 M NH_4NO_3 adjusted to pH 7.0 with 10 M NaOH is used as the electrolyte. It was found by Saterlay *et al.*[21] that use of this electrolyte gave sharp and reproducible signals for the stripping of MnO_2.

The cyclic voltammetry of 1 mM Mn^{2+} in 0.5 M NH_4NO_3 adjusted to pH 7.0 at a bare bppg electrode exhibits two oxidative waves not seen in the absence of Mn^{2+} (Fig. 6). The first oxidation peak occurs at +0.48 V and the second at +0.85 V. Scanning to +0.65 V confirms that the first peak at + 0.48 V (*vs.* SCE) is correlated to the reductive wave seen at +0.24 V (*vs.* SCE) in the reverse scan. This reductive peak occurs very close to the calculated potential (+0.28

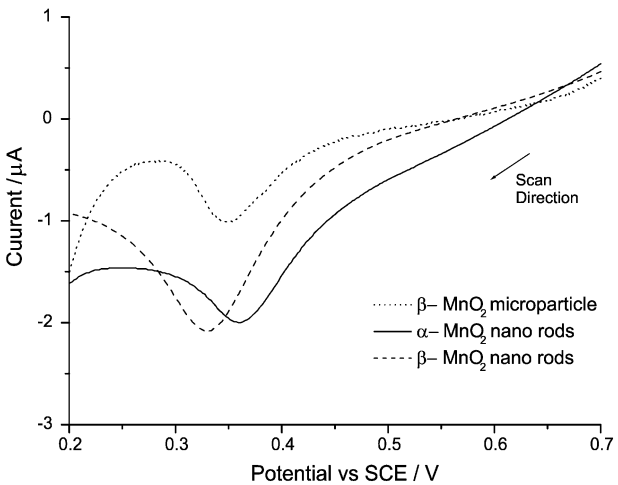

Fig. 5 Comparison of the LSVs of a bppg electrode modified with MnO_2 microparticles, α-MnO_2 nanorods and β-MnO_2 nanorods. Experiment run in 0.5 M NH_4NO_3 adjusted to pH 7.0 with 10 M NaOH. LSV ran at a scan rate of 10 mV/s

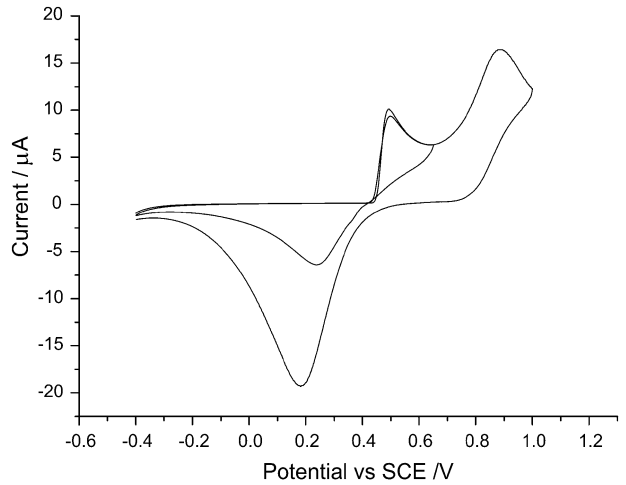

Fig. 6 The overlaid cyclic voltammograms (scan rate 10 mV/s) recorded over the range −0.4 V to +1.0 V and the second scan over the −0.4 V to +0.65 V region of a blank bppg electrode in a solution of 1 mM $Mn(ClO_4)_2$ and 0.5 M NH_4NO_3 adjusted to pH 7.0 with 10 M NaOH.

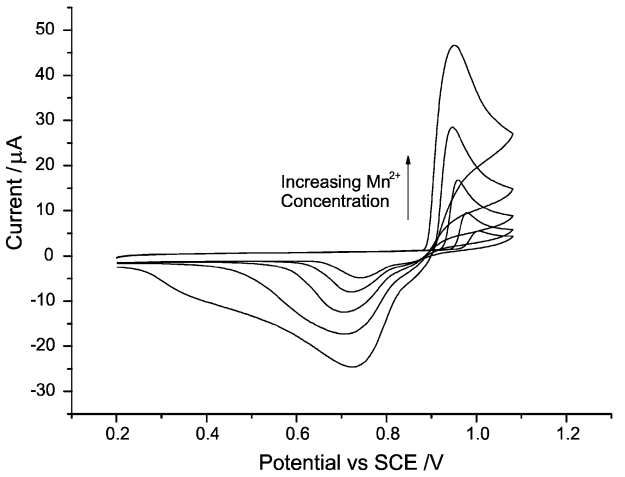

Fig. 7 The cyclic voltammetry (scan rate 10 mV/s) of a blank bppg electrode in the range of +0.2 V to +1.08 V. In a solution of varying concentrations of Mn^{2+} (0.1 mM, 0.2 mM, 0.4 mM, 0.8 mM and 1.6 mM) with a supporting electrolyte of 0.5 M NH_4NO_3 adjusted to pH 3.0 with HCl.

V) at which the reduction of MnO_2 to Mn^{2+} should occur. As such it maybe concluded that the wave at +0.48 V (*vs.* SCE) results in the production of MnO_2 on the surface of the electrode. If the oxidation of Mn^{2+} occurs *via* a direct two-electron process then from the Randles-Ševčík $i_p = (2.69 \times 10^5)n^{3/2}AD_0^{1/2}C^*_0v^{1/2}$ (where n is the number of electrons, A is the area of the electrode in cm^2, D_0 is the diffusion coefficient in $cm^2\ s^{-1}$, C^*_0 in the bulk solution concentration in mol/cm^3 and v is the scan rate in Vs^{-1}) then an estimation of the peak current maybe obtained if, in this first approximation we ignore that this process likely involves a nucleation-growth on the electrode surface as evidenced by the voltammetric wave shape. Taking the diffusion coefficient of Mn^{2+} to be 1.2×10^{-5} $cm^2\ s^{-1}$[26,27] then the peak current for the wave at +0.48 V (*vs.* SCE) is calculated to be 52.7 μA whilst the experimentally determined peak current is 9.17 μA; therefore the mechanism for MnO_2 deposition is almost certainly not a direct two electron process and the observed current is less than predicted by a diffusion only mechanism for reasons discussed below.

The presence of MnOOH as an intermediate in the electrodeposition of MnO_2 has been proposed before in other literature. Previously Clarke *et al.* undertook a detailed investigation into the electrodeposition of MnO_2 onto a Pt electrode.[28] From this work they were able to propose two main mechanisms of deposition one in low and one in high concentration of acid. In dilute acid (<1.0 M) they gave a mechanism that involved the production of Mn^{3+} which then undertook rapid hydrolysis to MnOOH. The use of MnOOH as the intermediate present was also suggested by Kao and Weibel whom proposed the growth of the deposited MnO_2 occurred by the reduction of MnO_2 by solution phase Mn^{2+} species.[4]

$$Mn^{2+} + MnO_2 + H^+ \rightarrow 2MnOOH + 2H^+ \qquad (2)$$

The MnOOH produced is then electrochemically oxidised to MnO_2 *via*

$$MnOOH \rightarrow MnO_2 + H^+ + e^- \qquad (3)$$

This overall gives a net gain of MnO_2.

At lower pH values, as in Fig. 7 where the solution was adjusted to pH 3.0 with HCl it is not possible to confirm the presence of a second peak primarily due the limitations of the electrochemical window. It is noted that at pH 3.0 the oxidative wave does not limit with increasing concentration of Mn^{2+} and that the reductive peak shows a shoulder which is not observed at lower pH's. Assuming this shoulder to be the back peak for the oxidative wave a potential of +0.936 V (*vs.* SCE) is obtained for the redox couple. The standard potential for the oxidation of Mn^{2+} to MnOOH is found to be $E^0 = 1.5$ V.[29]

$$MnOOH + 3H^+ + e^- \rightarrow Mn^{2+} + 2H_2O \qquad (4)$$

Correction of this standard potential for pH 3.0 gives $E = +0.904$ V (*vs.* SCE). This is in good agreement with the value obtained experimentally and as such allows for possible identification of the intermediate present at this pH.

The effect of varying the concentration of Mn^{2+} below 1.6 mM on the electrodeposition in NH_4NO_3 adjusted to pH 7.0 was investigated and is shown in Fig. 8. With concentrations up to 0.4 mM Mn^{2+} the first peak scales with the amount of manganese present in solution and no peak at higher potentials is observed. At concentrations higher than 0.4 mM Mn^{2+} the first peak current limits and a second peak at more positive potentials (+0.85 V) becomes visible the peak current of this peak increases with increases manganese(II) concentration. To ascertain if both of these oxidative processes contribute to the electrodeposition of MnO_2 cathodic LSV was performed at different concentrations (0.1 mM to 1.6 mM) of manganese(II). At each concentration two procedures were completed; first the potential was held at +0.65 V (*vs.* SCE) and then cathodically scanned from +0.65 V to −0.4 V.

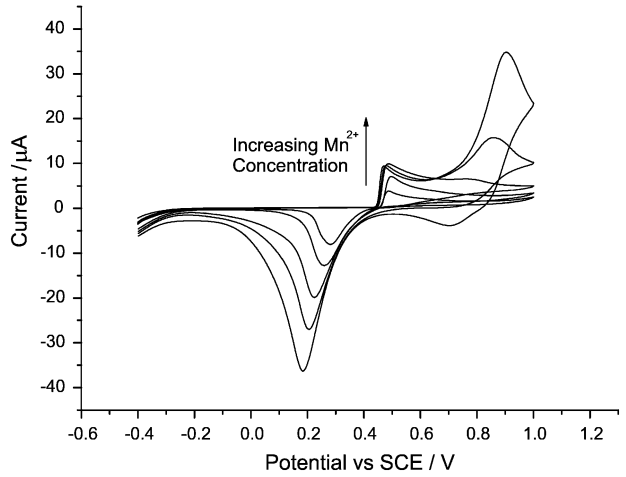

Fig. 8 The overlaid cyclic voltammagrams (scan rate 10 mV/s) of a blank bppg electrode in the range −0.4 V to +1.0 V with increasing concentrations of Mn^{2+} (0.1 mM, 0.2 mM, 0.4 mM, 0.8 mM and 1.6 mM). Experiment ran at 10mV/s in a 0.5 M NH_4NO_3 solution adjusted to pH 7.0 with 10 M NaOH.

Second the potential was held at +1.0 V (*vs.* SCE) and scanned in the cathodic direction from +1.0 V to −0.4 V (*vs.* SCE). The peak area of the MnO_2 stripping peak was then measured and plotted against the manganese(II) concentration. As can be seen from Fig. 9 when the system is conditioned at +0.65 V (*vs.* SCE) the stripping peak area increases and then limits at concentrations above 0.4 mM Mn^{2+}. This limiting behaviour is not observed when the system is conditioned at a potential that is greater than the peak +0.85 V (*vs.* SCE). Clearly both of the observed peaks are depositing manganese dioxide on to the electrode surface.

Assuming the mechanism for first oxidative peak to be as follows:

$$Mn^{2+} + 2H_2O \rightarrow MnOOH + 3H^+ + e^- \qquad (5)$$

followed by eqn (3). It may be postulated that the limiting current observed for the first peak above 0.4 mM Mn^{2+} in pH 7.0 adjusted 0.5 M NH_4NO_3 is due to the slow diffusion of the H^+ out of the MnOOH intermediate which may effect local changes in pH. This hypothesis is supported in work done by Kao and Weibel.[4] In high concentrations of Mn^{2+} they proposed that eqn (3) was the rate determining step for the deposition of MnO_2 with the in solid diffusion of H^+ through the produced MnOOH being the limiting factor. The proton diffusion coefficient was estimated as being similar to the diffusion coefficient of H^+ through MnO_2. A value of 2×10^{-15} cm^2 s^{-1} at 25 °C for this diffusion coefficient was found by reference to their previous work.[30] At lower concentrations the rate determining step is the diffusion of Mn^{2+} from bulk solution to the electrode *i.e.* eqn (5) is the rate limiting step.

The peak current for the oxidative wave found at +0.48 V (*vs.* SCE) was measured at varying scan rates. Fig. 10 shows the concentration and scan rate independent plot of peak current against scan rate for this data. If the diffusion coefficient[26,27] of the manganese(II) is taken as 1.2×10^{-5} cm^2 s^{-1} and it is assumed the oxidation is a one electron process then through use of the Randles–Ševčík equation a constant value of 186.4 A mol^{-1} cm^3 $s^{0.5}$ $V^{-0.5}$ is expected. As is seen from the plot this value is not followed for either of the low concentrations of Mn^{2+} plotted. At faster scan rates both of the plots approach the value predicted by the Randles–Ševčík equation. This behaviour is suggestive of either an ECE or a DISP process. If the process is taken to be an ECE mechanism in which a one electron transfer is followed by a chemical step from which the product of chemical step is oxidised further then at higher scan rates the chemical step will be out run and therefore the mechanism will tend to a one electron process. Alternatively if the mechanism is viewed as a disproportionation where a one electron process occurs and this intermediate then disproportionates at a given rate to yield then final product (in this case MnO_2), then also with this latter mechanism at higher scan rates the disproportionation step would be expected to be out run and also result in a one electron wave.

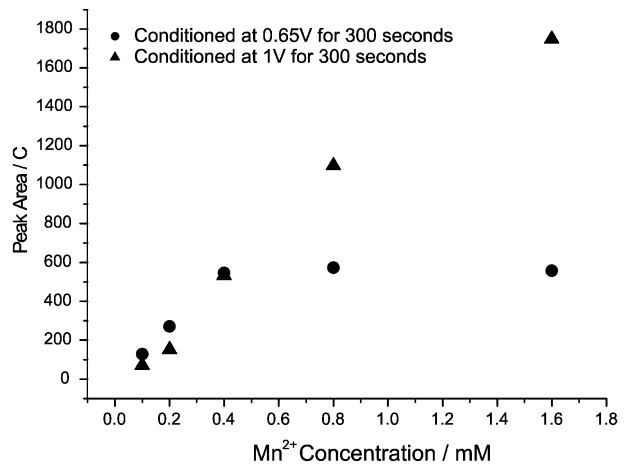

Fig. 9 Plot of the area of the MnO_2 stripping peak against manganese concentration with the system conditioned at either +0.65 V or +1.0 V. After conditioning of the system LSV is run in the cathodic direction at a scan rate of 10 mV/s.

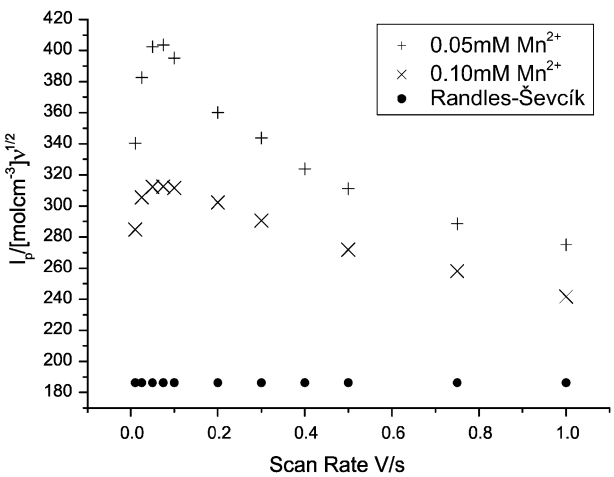

Fig. 10 Scan rate and concentration independent plot of peak current against scan rate for the peak found at +0.48 V. Peak current measured from CV's of a blank bppg electrode in 0.5 M NH_4NO_3 adjusted to pH 7.0 with 10 M NaOH. Experiment performed with 0.05 mM and 0.1 mM Mn^{2+}.

At lower scan rates if the deposition is occurring through a DISP or ECE process then the peak current would be expected to be closer to that of a two electron transfer. However below 50 mV s^{-1} the peak currents are less than would be expected if the mechanism was to be viewed as DISP or ECE process as can be seen in Fig. 10. The unusual plot shape of Fig. 10 maybe explained by use of the earlier proposed mechanism as described by eqn (3) and (4); at low scan rates a larger amount of MnOOH is deposited than at higher rates as such eqn (3) is the rate determining step but at higher scan rates where the deposited MnOOH layer is thinner the diffusion of Mn^{2+} to the surface is found to be the limiting factor.

It maybe speculated that at pH 3.0 a different mechanism for the oxidation of the MnOOH species is occurring. One explanation is found through the disproportionation of MnOOH to Mn^{2+} and MnO_2.

$$2MnOOH + 2H^+ \overset{K_{Disp}}{\rightleftharpoons} Mn^{2+} + MnO_2 + 2H_2O \qquad (6)$$

From the use of standard potentials[22] at pH 3.0 K_{disp} is found to be 2.2×10^6 but at pH 7.0 this value is reduced to 2.28×10^{-2}. As such at lower pHs the MnOOH intermediate is able to disproportionate whereas conversely at higher pH's it is less able to do so, due to the lack of available protons. Therefore at pH 7.0 the oxidation must proceed *via* the earlier proposed mechanism of a second electrochemical step as described by eqn (3). The ability of MnOOH to disproportionate at pH 3.0 means that the oxidation is not limited by the in diffusion of H^+ through the solid MnOOH layer.

The cyclic voltammetry of a solution containing 1.6 mM Mn^{2+} in 0.5 M NH_4NO_3 adjusted to pH 7.0 shows a back peak for the oxidative peak at +0.85 V. By comparison of the potential for the forward and back peak a value of $E = 0.801$ V for the redox couple is obtained. The standard potential for the oxidation of manganese(II) to manganese(VI) is $E^0 = +1.75$ V.[22]

$$Mn^{2+} + 4H_2O \rightarrow MnO_4^{2-} + 8H^+ + 4e^- \qquad (7)$$

Adjusted to pH 7.0 this give a potential of +0.797 V (*vs.* SCE) which is close to the value obtained experimentally. Duarte *et al.*[31] observed that on scanning past the Mn^{2+} oxidation peak a second oxidative process occurred but was partially obscured by the onset of solvent break down. They hypothesised this second peak was due to the oxidation of MnO_2 to soluble manganese(VII). However, we observe that the second peak in NH_4NO_3 adjusted to pH 7.0 has been shown to increase the quantity of deposited MnO_2, suggesting that the MnO_4^{2-} produced may then react with Mn^{2+} present at the electrode surface to form MnO_2 by eqn (8)

$$MnO_4^{2-} + Mn^{2+} \rightarrow 2MnO_2 \qquad (8)$$

The presence of MnOOH as the intermediate present in the electrodepostion of MnO_2 has been proposed due to the correlation of the peak position at pH 3.0 of the oxidative wave at +0.936 V with that expected through the use of standard electrode potentials. This is corroborated by the other authors in the literature whom also cite MnOOH as the intermediate species. At pH 7.0 a mechanism for the electrodeposition involving two electrochemical steps was suggested (eqn (3) and (4)). This proposed mechanism fits qualitatively well with the experimental data obtained, allowing an explanation for the observed limiting of the peak current of the oxidative wave present at +0.48 V (*vs.* SCE); the production of a layer of MnOOH causes eqn (3) becomes the rate determining step due to the slow diffusion of H^+ through the solid. Further to this an explanation for the second peak was also provided through the proposed production of MnO_4^{2-} which *via* eqn (8) forms more MnO_2. When the deposition of MnO_2 of is studied at pH 3.0 it is noted that the first oxidative wave at +1.00 V (*vs.* SCE) does not limit and it was proposed that at this pH an alternate method of deposition of MnO_2 is possible through the disproportionation of MnOOH. At higher pH's it was shown through the use of standard potentials that the disproportionation (as shown by eqn (6)) becomes less favourable.

3.4 The amperometric detection of hydrogen peroxide with MnO_2

As stated in the introduction, the detection of hydrogen peroxide been used in a number of biochemical sensors as the measurable analyte to provide an indirect but quantifiable measurement of other analytes.[18,19] As such the determination of hydrogen peroxide in aqueous solutions on manganese dioxide was examined using cyclic voltammetry in the range −0.4 V to +1.0 V (*vs.* SCE) at a bppg electrode modified with MnO_2 microparticles in 0.5 M NH_4NO_3 adjusted to pH 7.0. The first two overlaid scans are shown in Fig. 11. The oxidation peak at +0.42 V is attributed to the Mn(II)/Mn(IV) redox couple—eqn (1). Note that on repeat scans the size of this peak was found to gradually decrease. This observed decrease in peak current occurs due to being scanned at a potential below that of the Mn(II)/Mn(IV) redox couple *i.e.* below +0.28 V. At the start of the experiment manganese(II) is produced in the solution phase, this manganese(II) is subsequently reoxidised to manganese(IV) at a potential of +0.42 V (*vs.* SCE) and on the reverse scan the reduction of manganese(IV) to manganese(II) is observed. The decrease in size of the peaks on repeat scans suggests that the amount of manganese dioxide present on the electrode surface is reduced

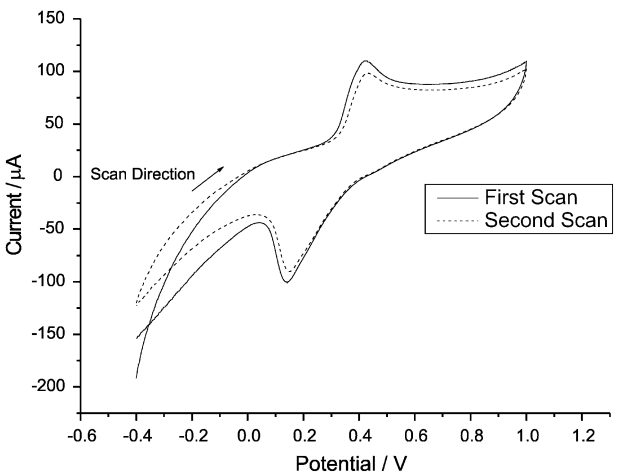

Fig. 11 The overlaid cyclic voltammagrams of a bppg electrode modified with MnO_2 microparticles in a solution of 0.5 M NH_4NO_3 adjusted to pH 7.0, run in the range −0.4 V to +1.0 V at a scan rate of 50 mV/s.

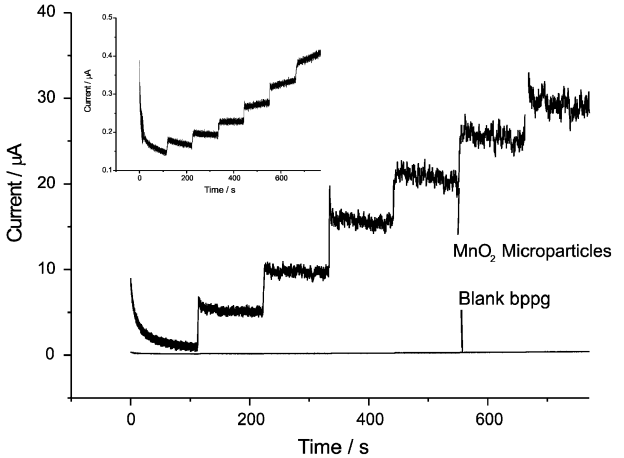

Fig. 12 A plot showing the chronoamperometric response for a blank bppg electrode and a bppg electrode modified with MnO_2 microparticles. Experiment was run in 0.5 M NH_4NO_3 adjusted to pH 7.0 with the potential held at +0.8 V (*vs.* SCE). The 100 μM addition of H_2O_2 every 110 seconds by standard addition. Inset shows the enlarged current-time plot for the blank bppg electrode.

or the surface of the MnO_2 microparticles is altered by the dissolution process. This behaviour precludes the possibility of using cyclic voltammetry to explore the analytical response of the MnO_2 materials towards H_2O_2.

To overcome the problem of MnO_2 dissolution we applied chronoamperometry to investigate the analytical performance of the MnO_2 microparticles, α-MnO_2 and β-MnO_2 nanorods towards H_2O_2. The amperometric response of a blank bppg electrode was compared to that of a bppg electrode modified with MnO_2 microparticles. The current was held at +0.8 V (*vs.* SCE) and every 110 seconds a standard 20 μl aliquot of 0.125 M H_2O_2 was added to 25 cm^3 solution of 0.5 M NH_4NO_3 adjusted to pH 7.0. This addition of H_2O_2 to the electrolyte consecutively increases the hydrogen peroxide concentration by 100 μM. Fig. 12 depicts the current-time response of the standard additions with the inset showing enlarged blank bppg plot. It is easily seen that the modified electrode shows a far greater response to the standard additions and it can therefore be assumed that the MnO_2 is catalytic for the oxidation of hydrogen peroxide compared to a bare carbon electrode. At higher concentrations of H_2O_2 the noise increases greatly, which we tentatively suggest is due to the formation of micro bubbles of oxygen from the oxidation of the peroxide at the electrode surface.

Fig. 13(a) depicts the amperometric response to increasing concentrations of H_2O_2 of the bppg electrode modified with MnO_2 microparticles the inset shows the standard addition plot. By applying a linear fit a correlation equation of $I_p(A) = 0.05442C + 3.498 \times 10^{-5}$ (where C is the concentration) is obtained with a related R^2 value of 0.996. The limit of detection (LOD) was determined through use of the 3 sigma method.[32] From this method the limit of detection is defined as a signal equal to three times the standard deviation:

$$\mathrm{LOD} = 3\sigma/b$$

Here σ is defined as the standard deviation of the y-coordinates from the line of best fit and b is the slope of the same line.

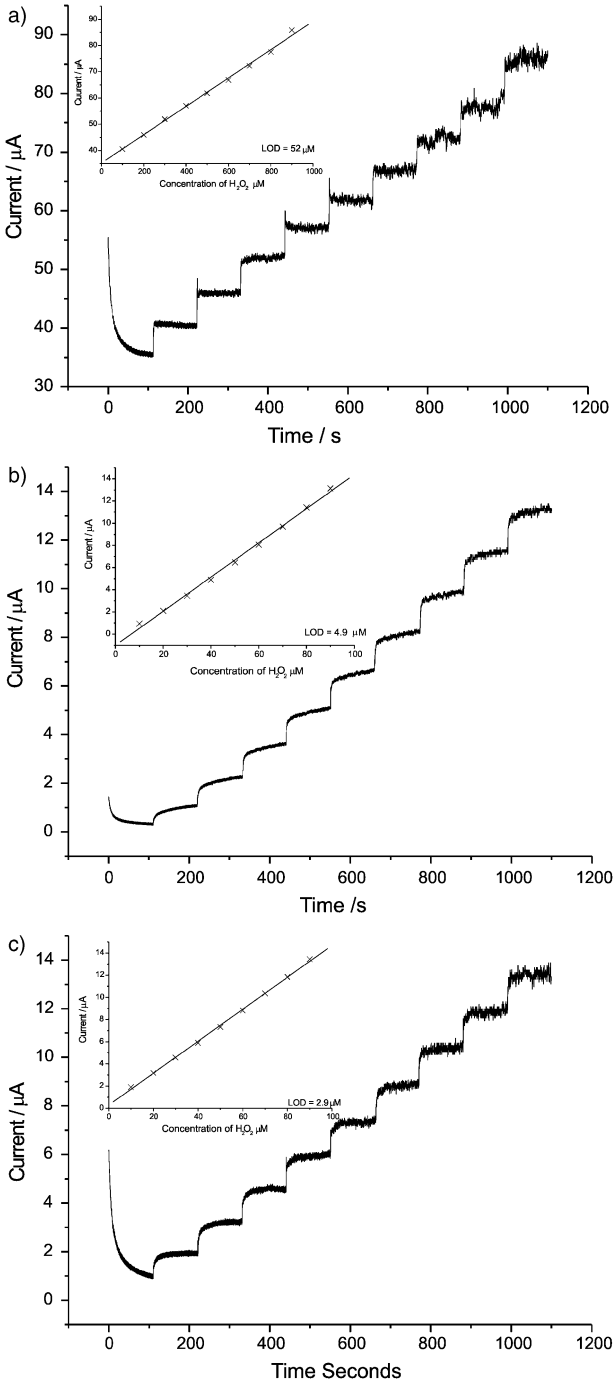

Fig. 13 (a) Shows the chronoamperometric response for a bppg electrode modified with MnO_2 microparticles in a 0.5 M NH_4NO_3 solution adjusted to pH 7.0. Standard additions of 20 μl of 0.125 M H_2O_2 were added to 25 cm^3 of electrolyte every 110 s. Inset shows the standard addition plot. (b) And (c) have smaller additions of H_2O_2 with the concentration being increased by 10 μM every 110 seconds. (b) Is a bppg electrode modified with alpha MnO_2 nanorods and (c) is a bppg electrode modified with beta MnO_2 nanorods.

From this the limit of detection of hydrogen peroxide through use of a bppg electrode modified with MnO_2 microparticles was 52 μM. Due to the method of attachment of the manganese dioxide microparticles used it was not possible to get a consistent coverage of manganese onto the electrode surface.

Therefore any repeat results show varying limits of detection, consequently use of this method for any analytical purpose requires electrode calibration.

The above experiment was repeated with both alpha- and beta-MnO_2 nanorods modified bppg electrodes but with lower standard additions of hydrogen peroxide (10 μM). The amperometric response of the alpha manganese dioxide to the standard additions of H_2O_2 is shown in Fig. 13(a) the LOD for this experiment was calculated to be 4.9 μM. Repeat experiments found limits of detection of 7.3 μM and 5.0 μM. Fig. 13(b) shows the time current response for a bppg electrode modified with beta manganese dioxide with additions of 20 μl of 0.0125 M H_2O_2 to 25 cm^3 of electrolyte every 110 seconds. The limit of detection for these experiments was found to be 2.9 μM subsequent repeat experiments found LOD's of 1.2 μM and 6.2 μM. By casting the manganese dioxide onto the electrode surface a more consistent electrode surface is produced.

Both of the manganese nanorods show far better limits of detection than for the microparticles. As mentioned in the introduction manganese dioxide suffers from low surface areas it is speculated that the improved amperometric detection for the manganese dioxide nanorods is in part due to their significantly larger surface area. Although not conclusive it does appear that the beta nanorods show a marginally lower limit of detection. If a mechanism for the catalytic oxidation of hydrogen peroxide by MnO_2 is envisaged to involve the reduction of the manganese dioxide to either Mn(III) or a Mn(II) species then the rate of catalysis may be governed by the relative ease of MnO_2 reduction *i.e.* at a reduced overpotential. As shown by Fig. 5, beta rods are reduced at a marginally lower potential than the alpha, subsequently this may provide them with a greater catalytic activity towards peroxide oxidation.

4. Conclusion

The electrodeposition of MnO_2 from a solution of Mn(II) has been investigated at physiological pH. At pH 7 the electrodeposition of MnO_2 proceeds *via* an ECE mechanism with the rate determining step likely to be the diffusion of protons out of a thin layer of MnOOH as an intermediate. At more positive potentials a further oxidative process, not previously definitively observed, occurs at *ca* +0.9 V *vs.* SCE whose potential corresponds to the formation of the MnO_4^{2-} species. This can further react with Mn(II) present in the solution to increase the amount of MnO_2 deposited onto the electrode surface.

The energetic difference between the alpha and beta phases of the MnO_2 nanorods was measured from the difference in the observed MnO_2 reduction peak potential and was found to be *ca.* 3 kJ mol^{-1}. A further difference in the observed reduction peak potential of the beta-phase nanorods and the beta-phase MnO_2 microparticles was also observed suggesting that there is a difference in the structural or surface energies of the nanometre-sized materials.

Finally the electrocatalytic behaviour of all three materials studied towards the analytical detection of hydrogen peroxide was studied. Both phases of the MnO_2 nanorods produced siginificantly lower limits of detection (*ca.* 5.0 ± 2.5 μM based on 3σ) and greater sensitivity towards hydrogen peroxide than the MnO_2 microparticles (*ca.* 50 ± 2 μM). This likely reflects the increased surface area of these materials but the different surface or structural energies of the nanometre-sized materials may also play a role as suggested by the slightly lower limit of detection found at the beta-MnO_2 nanorods compared to the alpha-MnO_2 nanorods.

Acknowledgements

GGW thanks St John's College, Oxford, for a Junior Research Fellowship. LS would like to thank Gerard Tobias for his supervision.

References

1. K.-J. Euler, *J. Power Sources*, 1982, **8**, 133.
2. S. Nijjer, J. Thonstad and G. M. Haarberg, *Electrochim. Acta*, 2000, **46**, 395.
3. H. Zhang and S. M. Park, *J. Electrochem. Soc.*, 1994, **141**, 2422.
4. W. H. Kao and V. J. Weibel, *J. Appl. Electrochem.*, 1992, **22**, 21.
5. Y. Chabre and J. Pannetier, *Prog. Solid St. Chem.*, 1995, **23**, 1.
6. V. G. Kumar and B. Kim Kwang, *Ultrason. Sonochem.*, 2006, **13**, 549.
7. C. Ye, Z. M. Lin and S. Z. Hui, *J. Electrochem. Soc.*, 2005, **152**, A1272.
8. B. Tang, G. Wang, L. Zhuo and J. Ge, in *'Method for preparing dandelion-like and rod-like manganese dioxide nanomaterial by hydrothermal reaction'*, Application: CN1004-3204 1686826, 2005.
9. Y. Bando, T. Sasaki and R.-C. Ma, in *'Layered manganese dioxide nano-belt and its manufacture'*, Application: JP2004-133154 20053141522005.
10. S. Turner and P. R. Buseck, *Science*, 1981, **212**, 1024.
11. S. Bakardjieva, T. Grygar and P. Vorm, *J. Solid State Electrochem.*, 2000, **4**, 306.
12. J. C. L. J. Chen, V. Purohit, M. B. Cutlip and S. L. Suib, *Catal. Today*, 1997, **33**, 205.
13. G. G. Xia, Y. G. Yin, W. S. Willis, J. Y. Wang and S. L. Suib, *J. Catal.*, 1999, **185**, 91.
14. G. Qi and R. T. Yang, *Appl. Catal.*, 2003, **44**, 217.
15. C. E. Langley, B. Šljukić, C. E. Banks and R. G. Compton, *Anal. Sci.*, 2007, **23**, 165.
16. N. Keren, M. J. Kidd, J. E. Penner-Hahn and H. B. Pakrasi, *Biochem.*, 2002, **41**, 15085.
17. O. M. S. Filipe and C. M. A. Brett, *Talanta*, 2003, **61**, 643.
18. M. D. Rubianes and G. A. Rivas, *Electroanalysis*, 2005, **17**, 73.
19. M. D. Rubianes and G. A. Rivas, *Electrochem. Commun.*, 2003, **5**, 689.
20. X.-C. Song, Y.-F. Zheng, S. Lin and Y. Wang, *Acta Phys.-Chim. Sin.*, 2007, **23**(2), 258.
21. A. J. Saterlay, J. S. Foord and R. G. Compton, *Analyst*, 1999, **124**, 1791.
22. A. J. Bard, *'Standard Potentials in Aqueous Solution'*, Marcel Dekker Ltd, New York, 1985.
23. W. C. Maskell, *J. Electroanal. Chem.*, 1986, **199**, 127.
24. K. Schachl, H. Alemu, K. Kalcher, H. Moderegger, I. Svancara and K. Vytras, *J. Anal. Chem.*, 1998, **362**, 194.
25. E. Turkusic, V. Milicevic, H. Tahmiscija, M. Vehabovic, S. Basic and V. Amidzic, *J. Anal. Chem.*, 2000, **368**, 466.
26. V. M. M. Lobo, *Pure and Appl. Chem.*, 1993, **65**, 2613.
27. J. A. Rard and D. G. Miller, *J. Solution Chem.*, 1985, **14**, 271.
28. C. J. Clarke, G. J. Browning and S. W. Donne, *Electrochim. Acta*, 2006, **51**, 5773.
29. D. L. Sparks, *'Environmental Soil Chemistry'*, Academic Press, London, 2003.
30. W. H. Kao, *J. Electrochem. Soc.*, 1988, **135**, 1317.
31. M. M. E. Duarte, A. S. Pilla and C. E. Mayer, *J. Appl. Electrochem.*, 2003, **33**, 387.
32. C. M. A. Brett and A. M. O. Brett, *'Electroanalysis'*, Oxford University Press, Oxford, 1998.